Deep Resources Engineering 2 (2025) 100168

Contents lists available at ScienceDirect

Deep Resources Engineering

journal homepage: www.keaipublishing.com/en/journals/deepre/

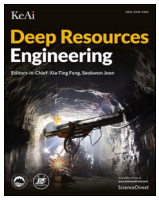

Full Length Article

Quantifying the mechanical properties of coal matrix and cleat using digital image correlation method

Yixiao Huang [a], Zhang Shi [a,b], Jimmy Li [a], Tiancheng Zhang [a], Zhongwei Chen [a,*]

[a] School of Mechanical and Mining Engineering, The University of Queensland, St Lucia, QLD 4072, Australia
[b] Specialist Testing Department, Alliance Geotechnical Pty. Ltd, Seven Hills, NSW 2147, Australia

ARTICLE INFO

Keywords:
Digital image correlation
Non-contacting video extensometer
Cleat networks
Young's modulus
Cleat compressibility

ABSTRACT

Coal mass consists of matrices and cleats, which exhibits significant difference in mechanical properties, such as uniaxial compressive strength and Young's modulus. Understanding this difference is critical for a number of engineering applications, such as assessing the stability of cleated coal seam gas wellbores, underground excavation stability in coal seams, and estimating cleat aperture response during gas extraction and surface response to reservoir depletion. The conventional method of measuring coal mechanical properties using strain gauges or displacement transducers is impractical and unreliable as it only captures the value for the installed point. This study explores the use of a two-dimensional Digital Image Correlation (2D-DIC) method to quantify the areal deformation of coal matrix and cleat regions and their contribution to the bulk mechanical properties of coal. Cyclic uniaxial compression tests were performed on coal specimens from the Goonyella Middle Seam, Australia. The results from the DIC technique were initially validated against strain gauge and Advanced Video Extensometer (AVE) measurements, showing minimal percentage differences: 5 % with the strain gauge; 16.6 % with the coal cleat region, 12.03 % with the coal matrix region, and 9.28 % with the coal bulk region compared to AVE. These results demonstrate that DIC is a reliable and accurate method for measuring coal deformation. Comparative analysis of cleat, matrix, and overall coal surface regions revealed distinct variations in Young's modulus, with ratios of E_{cleat}:E_{matrix}:$E_{overall}$ = 0.24:1.60:1.00. The calculated cleat and matrix moduli are 143.6 MPa and 1785.3 MPa respectively. The contributions of E_{matrix} and E_{cleat} to the overall Young's modulus ($E_{overall}$) were quantified, revealing that the matrix accounts for 56 % (A = 0.56) and the cleat for 44 % (1 - A = 0.44) of the overall modulus. The compressibility of the cleat shows six times that of the coal matrix (C_{cleat}: C_{matrix}:$C_{overall}$ = 4.24: 0.62: 1.00), highlighting the critical role of cleats in coal deformation and stress-induced permeability changes. Furthermore, Poisson's ratios computed from the DIC for the tested coal samples range from 0.19 to 0.33, showing strong agreement with reported values in the literature. By integrating DIC analysis with traditional mechanical testing, this study offers a robust approach to evaluating full-field deformation mechanisms in fractured materials. These findings advance the understanding of coal's mechanical properties, which in turn supports more accurate geotechnical modeling, optimizes mining design, and enhances coal seam gas extraction strategies.

1. Introduction

Coal is a naturally heterogeneous and anisotropic medium, resulting in complex mechanical behavior under external loading conditions, which can significantly affect its structural integrity [13]. Understanding these mechanical properties is essential for applications, such as assessing the stability of coal seam gas wellbores [7,18] and excavation stability in underground mining (e.g., pillars and roadways) [9]. Consequently, there is a need to develop robust methodologies for accurately quantifying the mechanical properties of each component, including coal matrix, cleat and bulk.

The mechanical behavior of coal is predominantly influenced by its matrix and cleat networks. Cleats, which are natural fractures within coal beds, provide pathways for stress redistribution and deformation, significantly impacting the strength, the cleat elasticity, and the cleat aperture response to reservoir depletion. Extensive research has been undertaken to investigate how cleats affect the bulk mechanical performance of coal. For example, Hou et al. [8] demonstrated that cleat

* Corresponding author.
E-mail address: zhongwei.chen@uq.edu.au (Z. Chen).

https://doi.org/10.1016/j.deepre.2025.100168
Received 16 December 2024; Received in revised form 8 February 2025; Accepted 19 February 2025
Available online 27 February 2025

Table 1
Comparison of popular methods for studying coal properties and deformation.

Method	Description	Advantages	Limitations	Reference
Strain Gauge	Uses electrical resistance changes in a bonded sensor to measure strain.	High precision, well-established	Limited to point measurements, cannot capture full-field strain, prone to damage under harsh conditions.	[4,10]
Digital Image Correlation (DIC)	Optical method that tracks surface deformation by analyzing a speckled pattern in sequential images	Full-field strain and displacement mapping, non-contact method, adaptable for complex geometries.	Requires high-quality imaging equipment, sensitive to lighting and surface preparation.	[4,6,19]
Video-Extensometer	Optical extensometer that tracks gauge marks	Non-contact, simple setup	Limited to linear strain along gauge marks, cannot measure fellfield deformation	[17]
Acoustic Emission	Captures stress-induced micro-cracking events by detecting high-frequency waves generated within the material.	Provides insight into fracture initiation and propagation.	Cannot measure strain directly, requires complementary methods for strain or displacement analysis.	[16]
Ultrasonic Velocity Measurement	Measures changes in wave velocities through the material	Non-destructive, provides indirect insights into material properties.	Indirect measurement, no direct strain mapping.	[3]

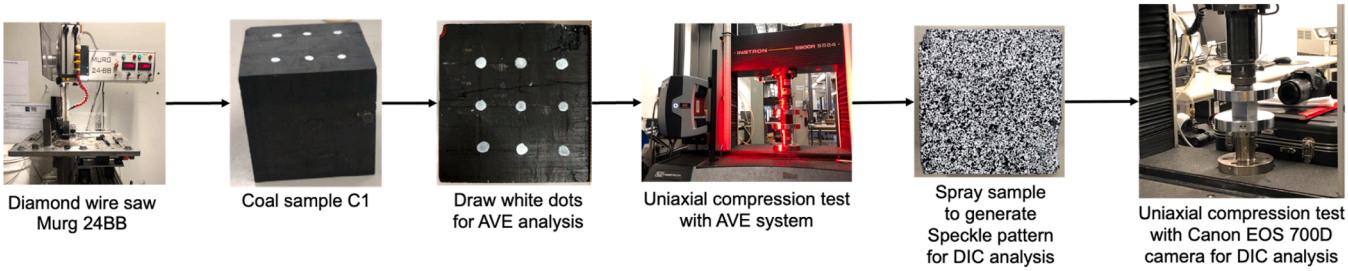

Fig. 1. Experimental flowchart.

complexity, quantified by fractal dimensions, significantly influences mechanical properties. They observed that uniaxial compressive strength and Young's modulus decrease with increasing cleat complexity. Similarly, Bin et al. [1] identified directional differences in tensile and compressive strengths relative to bedding planes, with vertical-direction strengths generally lower and more variable than parallel-direction strengths. Furthermore, Hao et al. [5] employed scanning electron microscopy, uniaxial compression tests, and acoustic emission monitoring to study hard coal with varying bedding and cleat angles. Their findings revealed that coal specimens exhibited the lowest peak strength when the bedding and face cleat dip angles were 45° and the butt cleat dip angle was 90°. Overall, these studies highlight the critical role of cleat geometry and orientation in determining the mechanical properties of coal. However, there is still a lack of research that directly determines the contribution of coal cleat and matrix deformation to the overall coal mechanical properties.

To address this, it is essential to employ alternative testing methods, which are capable of capturing the contributions of both matrix and cleat network deformation to coal bulk response. The complex coal cleat network can result in different deformation behavior in different coal regions. Table 1 compares some widely used techniques for investigating coal properties and deformation. In general, traditional strain measurement methods, such as strain gauges and video extensometers, are often unsuitable for coal samples as they are limited to measuring strain in small, localized regions. Other techniques, like acoustic emission or ultrasonic velocity measurement, offer valuable insights into fracture initiation and propagation but cannot directly measure strain. In contrast, combining uniaxial compression tests with high-resolution, full-field strain measurement tools like Digital Image Correlation (DIC) could provide a comprehensive understanding of the areal deformation behavior of coal.

DIC has been widely used in non-contact deformation and strain measurement [14]. A growing number of studies use the DIC technique to investigate rock behavior in uniaxial and triaxial compression tests, as well as Brazilian tensile tests [15,20,22]. The method can capture strain localization, crack propagation, and energy evolution during rock failure [22]. Xing et al. [23] studied the rock fracture characteristics under dynamic compression using the DIC method. The strain recovery was detected in the post-peak stage, which cannot be detected using traditional strain measurement methods such as strain gauges. Chai et al. [2] investigated the rock-like samples' full-field damage and deformation characteristics under a uniaxial compression test using the DIC method. Based on the full-field deformation data, a damage variable was then proposed to characterize the damage introduced during the compression. The DIC has also been used in large-scale simulations of rock-like materials to observe overlying strata movement and fracturing during excavation [12]. The technique offers advantages over traditional measurement methods, providing continuous, non-contact measurements with high accuracy.

The DIC method is also widely adopted to investigate the mechanical behavior of coal. For example, to overcome the limitation of strain gauge, such as misplacement and localized measurements, Yang et al. [24] evaluated the applicability of DIC on Brazilian disc-shaped coal specimens and concluded that it provides a simpler and more effective approach for determining Young's modulus and Poisson's ratio. Similarly, Tan et al. [21] examined damage evolution in water-saturated coal under cyclic loading, demonstrating that resistivity and DIC responses exhibit consistent and complementary trends.

Despite extensive applications of the DIC technique for analyzing full-field deformation in materials such as rocks and coal, its application in distinguishing the strain behavior of cleat and matrix regions remains limited. Moreover, few studies have quantitatively assessed the contribution of cleats to overall coal deformation under compression.

To address these gaps, this study employs DIC to measure the full-field deformation of coal samples during cyclic compression tests, providing a detailed assessment of strain distribution in cleat and matrix regions and their respective contributions to bulk coal deformation. It also offers a quantitative comparison of cleat, matrix, and overall mechanical properties, enhancing the understanding of how cleats influence coal's mechanical behavior.

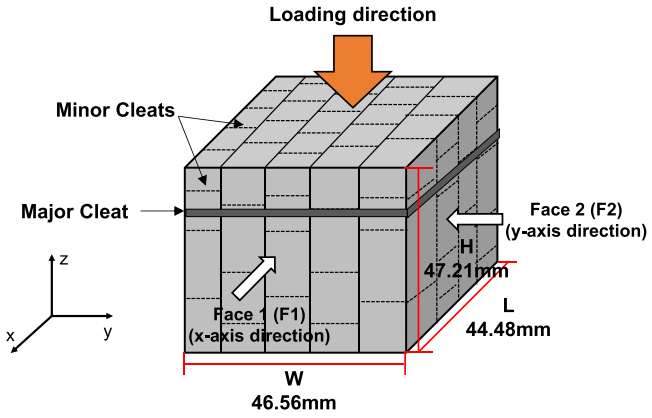

Fig. 2. Illustration of the cubic sample C1.

2. Testing setup and data analysis methodology

This section presents the experimental methodology and data analysis techniques. It begins with the preparation of coal samples and the description of the experimental setup. The data analysis process is then outlined, focusing on deriving Young's modulus and Poisson's ratio from Digital Image Correlation (DIC) data.

2.1. Testing methodology

Fig. 1 shows the experimental flowchart. Firstly, a coal lump from Goonyella Middle Seam in Bowen Basin, Australia, was prepared into a cubic sample (named C1) with 45 mm dimensions using a Diamond Wire Saw. The detailed sample dimensions and orientations are summarized in Fig. 2. The sample features a major cleat oriented along the y-axis, perpendicular to the loading direction. Minor cleats are randomly distributed throughout the sample, with the majority aligned along the y-axis.

Then, the uniaxial compression test was performed, with the loading applied along the z-axis, as shown in Fig. 2. Due to the limitation of the Instron machine, the AVE and DIC systems could not run simultaneously. Alternatively, two tests were conducted separately with the same uniaxial compression test settings, first with the AVE system and second time with the DIC system.

Instron 5900R-5584 machine is used to conduct cyclic uniaxial compression tests in this study. Due to the complex porous structure of the coal sample, significant gaps between the fractures could result in a large deformation during the first loading stage due to the sudden fracture closure. Therefore, cyclic loadings are performed to eliminate deformation. The loading/unloading rate was set up to be 500 N/min to ensure the surface deformation is slow enough to be captured by both AVE and DIC systems. The load was limited to 950 N to ensure the coal sample had a purely elastic deformation. The illustration of the loading and unloading cycles is shown in Fig. 3.

The Advanced Video Extensometer (AVE), a non-contacting strain measurement system, was first employed to determine the deformation during the uniaxial compression test [11] and is used as a benchmark to test the accuracy of the DIC method. The system records the variation of gauge length between marked points (see Fig. 4) using a high-resolution

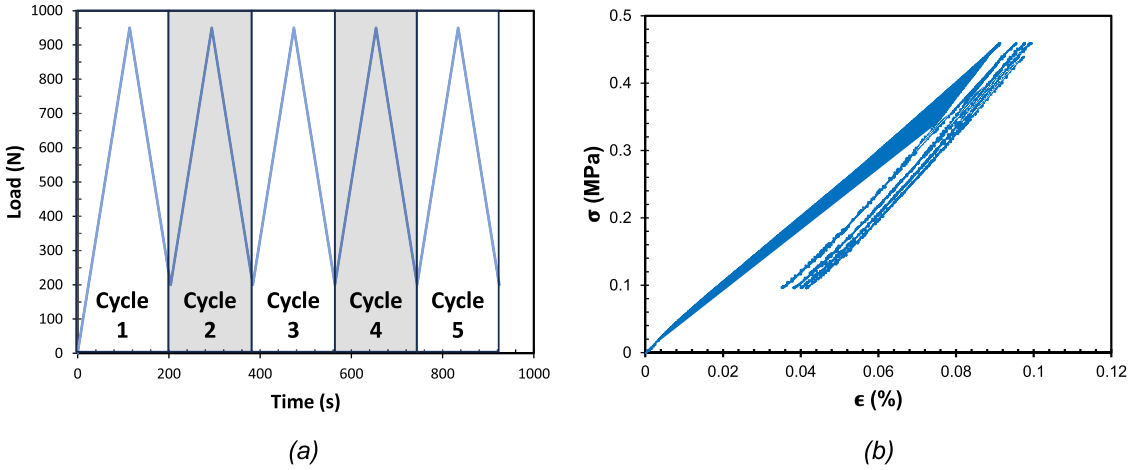

Fig. 3. Illustration of cyclic compression test loading sequence, (a) Load-Time and (b) Stress-Strain response from Instron 5900R-5584 during cyclic compression test.

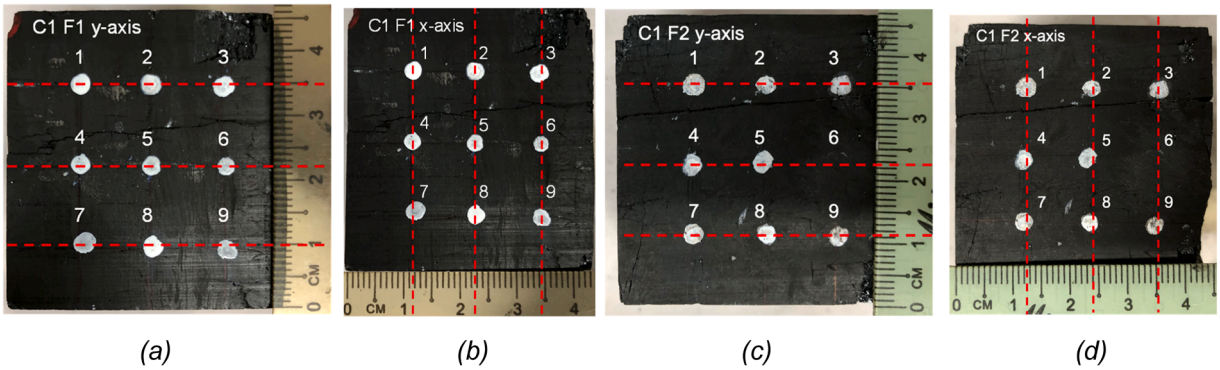

Fig. 4. C1F1 with white dots for AVE analysis (a) y-axis position (b) x-axis position; C1F2 with white dots for AVE analysis (c) y-axis position (d) x-axis position.

Table 2
AVE dot position with axes origin at the bottom-left corner of the sample (Refer toFig. 4).

	Position	1	2	3	4	5	6	7	8	9
C1 F1	Y (mm)	35.0	35.0	35.0	22.0	22.0	22.0	10.0	10.0	10.0
	X (mm)	11.5	22.5	34.0	11.5	22.5	34.0	11.5	22.5	34.0
C1 F2	Y (mm)	35.5	35.5	35.5	22.5	22.5	22.5	11.5	11.5	11.5
	X (mm)	12.5	24.0	35.0	12.5	24.0	35.0	12.5	24.0	35.0

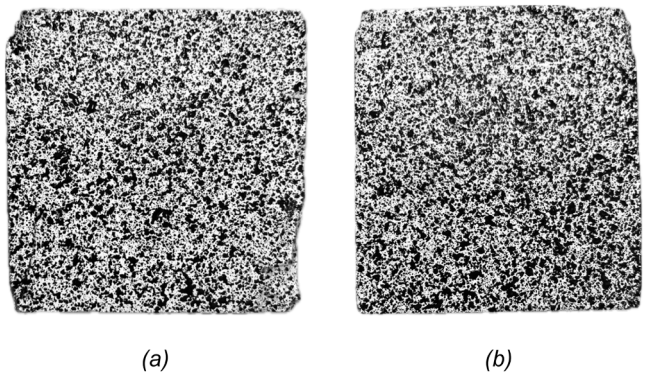

Fig. 5. (a) C1F1 with speckle patterns for AVE analysis; (b) C1F2 with speckle patterns for AVE analysis.

Table 3
DIC speckle pattern information.

	C1F1	C1F2
Density (black area/sample area)	0.32	0.32
Average black dots area (mm^2)	0.10	0.09
Average black dots dimension (mm)	0.53	0.43
Average black dots dimension (pixel)	11.21	9.44

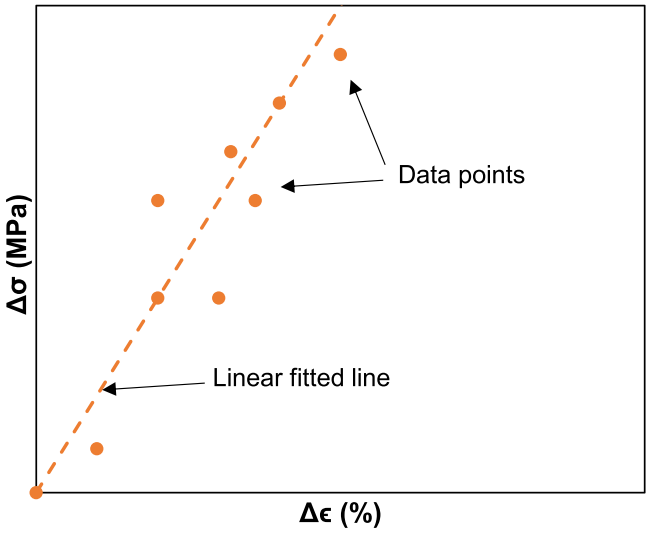

Fig. 6. Illustration of the stress-strain graph with $\Delta\sigma$ Vs. $\Delta\epsilon$ format.

digital camera and then calculates strain change over time by comparing the variation between these two dots. White dots were drawn on two surfaces of the sample, namely Face 1 (F1) and Face 2 (F2), for AVE analysis using the cyclic uniaxial compression test, and their information is summarized in Fig. 4 and Table 2.

After the compression test using the AVE system, speckle patterns were generated on the same surface of the sample for DIC analysis. To prepare the surface, the white dots from the previous test were first covered using Rust-Oleum Ultra Cover 2X primer paint. Then, speckle patterns were generated on the same surface using Wagon Black Paint and a spray gun. Fig. 5 illustrates the speckle patterns for samples C1F1 and C1F2, while Table 3 summarizes the speckle pattern density, average black dot area, and average black dot dimensions. It is important to note that the quality of the speckle pattern is crucial for achieving accurate DIC measurements. The subset size—defined as the area of a group of pixels used to track displacements between images—must be carefully selected to optimize performance. The subset size should be large enough for the software to distinguish distinct clusters (black and white regions) within the speckle pattern. In this study, a subset size of 29 pixels with a step size of 7 pixels was determined using VIC-2D software as the optimal configuration for the specific speckle pattern used in DIC analysis.

After the patterns were generated, the uniaxial compression test was performed with the DIC system. Canon EOS 700D single-lens camera was used to record images for DIC analysis with a 25 FPS frame rate and 1080p resolution. The video was then split into frames, and one frame was extracted from every 100 frames for analysis (frames with an interval for every 4 seconds).

2.2. Data analysis methodology

2.2.1. Stress-strain from cyclic uniaxial compression test

The Instron 5584 machine performs loading up to 950 N, then unloading to 200 N. This means that at the beginning of the next loading cycle, the sample will not recover back to its original strain (e.g., 0) due to the extra load supplied on the sample. Hence, for better comparisons between each loading cycle, the initial strain should be eliminated by introducing strain change $\Delta\epsilon$ and stress change $\Delta\sigma$ as:

$$\Delta\sigma = \sigma_{current} - \sigma_{initial} \tag{1}$$

$$\Delta\varepsilon = \varepsilon_{current} - \varepsilon_{initial} \tag{2}$$

where $\sigma_{current}$ is the current stress data, and $\sigma_{initial}$ is the stress at the start of the loading cycle. Similarly, $\varepsilon_{current}$ is the current strain data, and $\varepsilon_{initial}$ is the strain at the start of the loading cycle. Hence the stress-strain graph will be represented as $\Delta\sigma$ Vs. $\Delta\varepsilon$ as illustrated in Fig. 6.

2.2.2. Strain determination using the DIC method

With the help of the DIC method, the strain of each position on the surface of the sample can be identified and stored in a cartesian coordinate (e.g., position (2,3) ->$\varepsilon_{yy} = 0.0003$, $\varepsilon_{xx} = -0.0001$).

The strain of the selected region can be calculated by averaging the strains of all points within the region:

$$\varepsilon_{yy\ average} = \frac{\sum_{1}^{n} \varepsilon_{yy}}{n} \tag{3}$$

$$\varepsilon_{xx\ average} = \frac{\sum_{1}^{n} \varepsilon_{xx}}{n} \tag{4}$$

where $\varepsilon_{yy\ average}$ is the averaged strain along the y-axis (the forcing direction), $\varepsilon_{xx\ average}$ is the averaged strain along the x-axis, n is the number of points within the selected region in cartesian coordinate representation, ε_{yy} is the strain along the y-axis for each point, and ϵ_{xx} is the strain

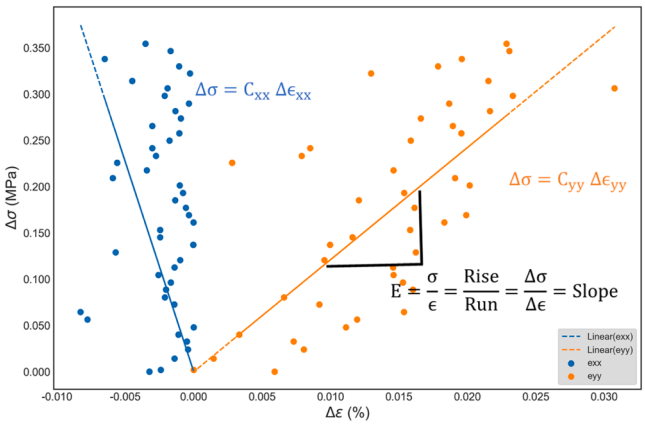

Fig. 7. Determine Young's modulus and Poisson's ratio using DIC data.

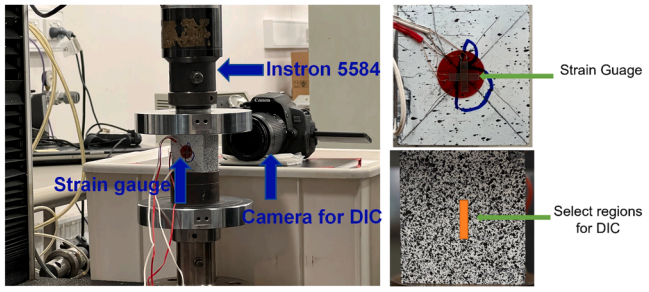

Fig. 8. Experimental setup of DIC accuracy validation with strain gauge method.

along x-axis for each point.

2.2.3. Young's modulus determination

Young's modulus can be defined as the slope of a stress-strain curve for a uniaxial compression test as illustrated in Fig. 7.

$$E = \frac{\sigma}{\varepsilon} = \frac{Rise}{Run} = \frac{\Delta\sigma}{\Delta\varepsilon} = slope \tag{5}$$

where $\Delta\sigma = \sigma_2 - \sigma_1$, is the stress change during a specific period, $\Delta\varepsilon = \varepsilon_2 - \varepsilon_1$ is the strain change in the period. Since the cyclic uniaxial compression test is performed, the period for $\Delta\sigma$ and $\Delta\epsilon$ is defined as the time when a loading cycle starts, to the time when it ends.

$$\Delta\sigma = \sigma_{end} - \sigma_{initial} \tag{6}$$

$$\Delta\varepsilon = \varepsilon_{end} - \varepsilon_{initial} \tag{7}$$

Young's modulus for each loading cycle can be determined using Eq. (5), Eq.(6) and Eq.(7).

2.2.4. Poisson's ratio determination

The Poisson's ratio can be calculated as the ratio of strain change, which can be expressed as:

$$\mu = -\frac{\varepsilon_{xx}}{\varepsilon_{yy}} = -\frac{\Delta\varepsilon_{xx}}{\Delta\varepsilon_{yy}} \tag{8}$$

The other way to determine Poisson's ratio is by using the ratio of the slope of the stress-strain curve. Similar to the method discussed in Young's modulus determination section, the slope can be obtained using the following formula:

$$Slope = \frac{\Delta\sigma}{\Delta\varepsilon} \tag{9}$$

The slope in Fig. 7 is represented as the coefficient C_{yy} and C_{xx} for ε_{yy} and ε_{xx}, respectively. Thus, the stress-strain curve can be expressed as:

$$\Delta\sigma = C_{yy}\Delta\epsilon_{yy} \tag{10}$$

$$\Delta\sigma = C_{xx}\Delta\epsilon_{xx} \tag{11}$$

Rearranging the above equations to obtain the expression for $\Delta\epsilon_{yy}$ and $\Delta\epsilon_{xx}$ as:

$$\Delta\varepsilon_{yy} = \frac{\Delta\sigma}{C_{yy}} \tag{12}$$

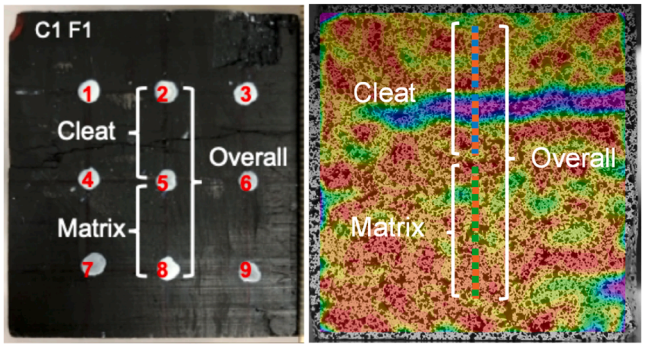

Fig. 10. Illustration of (a) AVE points and (b) DIC positions for C1F1.

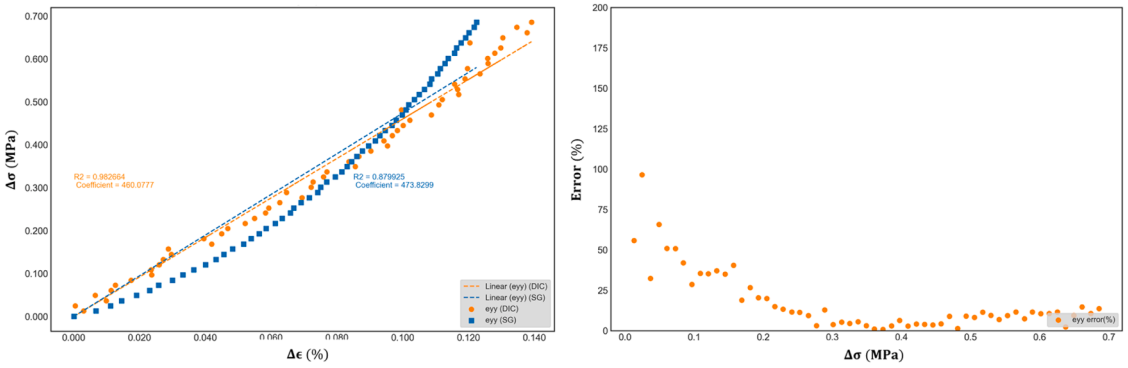

Fig. 9. (a) C2 delta stress ($\Delta\sigma$) Vs. delta strain ($\Delta\epsilon$) (DIC Vs strain gauge); (b) the percentage error between the DIC and strain gauge measurement.

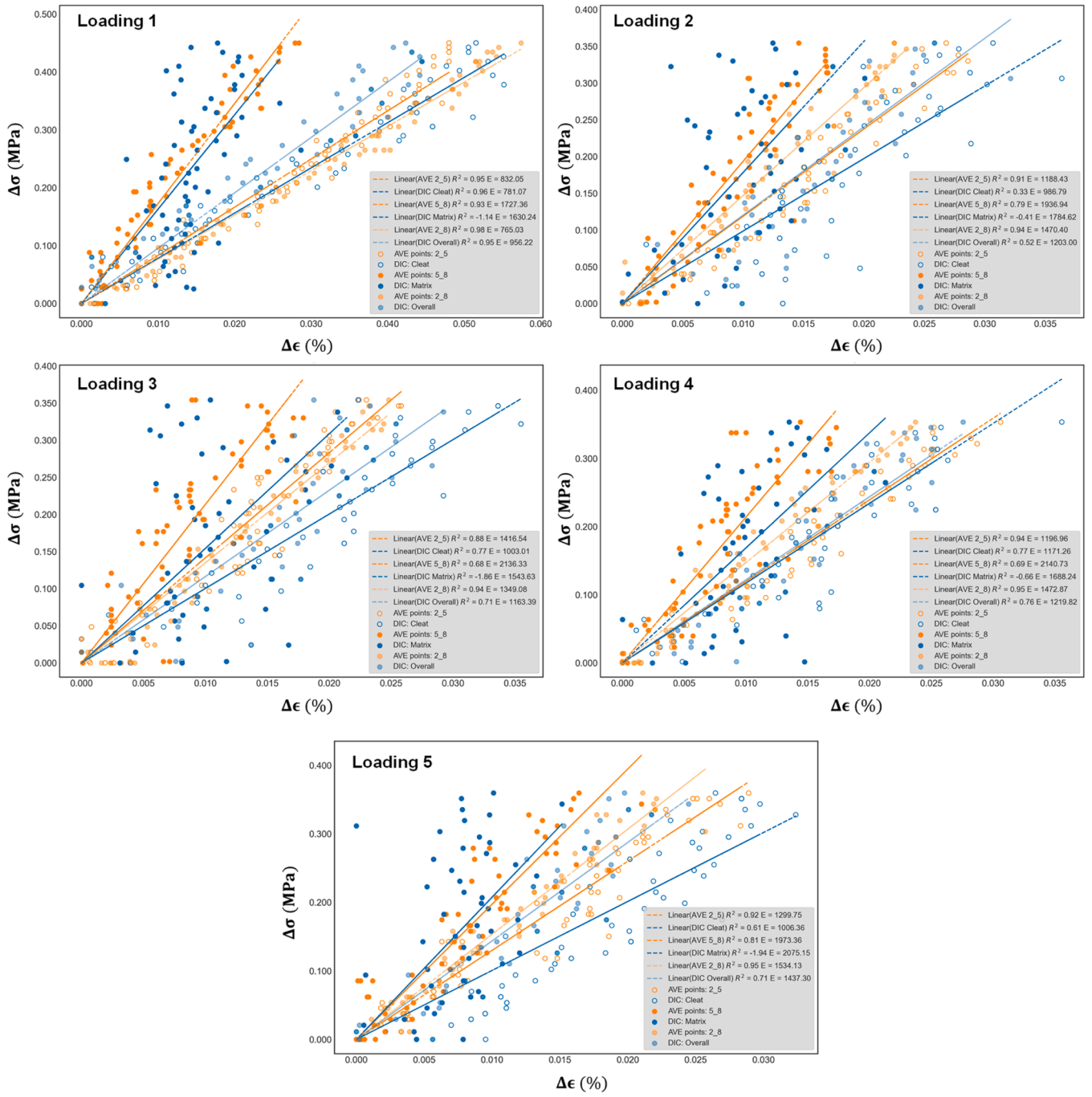

Fig. 11. C1F1 delta stress ($\Delta\sigma$) Vs. delta strain ($\Delta\epsilon$) for each loading cycle (DIC Vs AVE).

$$\Delta\varepsilon_{xx} = \frac{\Delta\sigma}{C_{xx}} \tag{13}$$

Then apply Eq.(8) to calculate the Poisson's ratio as:

$$\mu = -\frac{\Delta\varepsilon_{xx}}{\Delta\varepsilon_{yy}} = \frac{\frac{\Delta\sigma}{C_{xx}}}{\frac{\Delta\sigma}{C_{yy}}} = \frac{C_{yy}}{C_{xx}} \tag{14}$$

3. Results and analysis

This section presents the results from the DIC analysis. Firstly, the accuracy of the DIC method is validated using two methods: (i) strain gauge vs DIC results and (ii) AVE vs. DIC results. Then the DIC method was applied to determine the mechanical properties of both coal cleat and matrix systems.

3.1. DIC accuracy validation using strain gauge method

Since sample C1 has numerous small surface cleats that could affect strain gauge readings, another coal sample (named C2) without major cleats or fractures was used for verifying the accuracy of strain gauge and DIC measurements. Sample C2 was sourced from the same region as sample C1 and had identical dimensions. As shown in Fig. 8, a strain gauge (Tokyo Measuring Instruments Lab FCAB-5–11–1LJB-F) was attached to the center of one surface of the sample, while the DIC system was positioned on the opposite side to simultaneously monitor the vertical deformation of the central region during the compression test. The same Instron machine settings were applied, with the loading rate

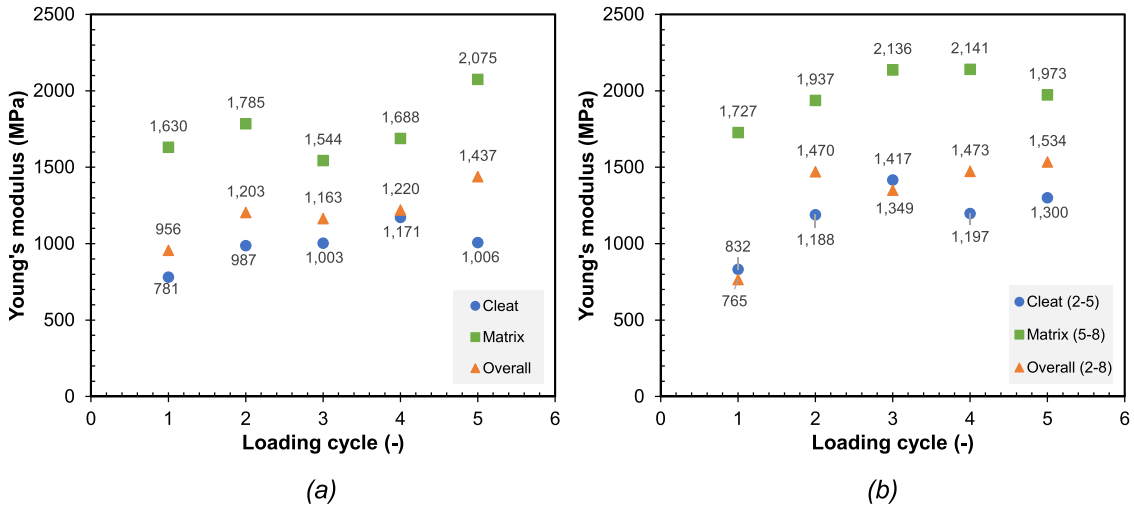

Fig. 12. Young's modulus of sample C1F1 from a) DIC and b) AVE.

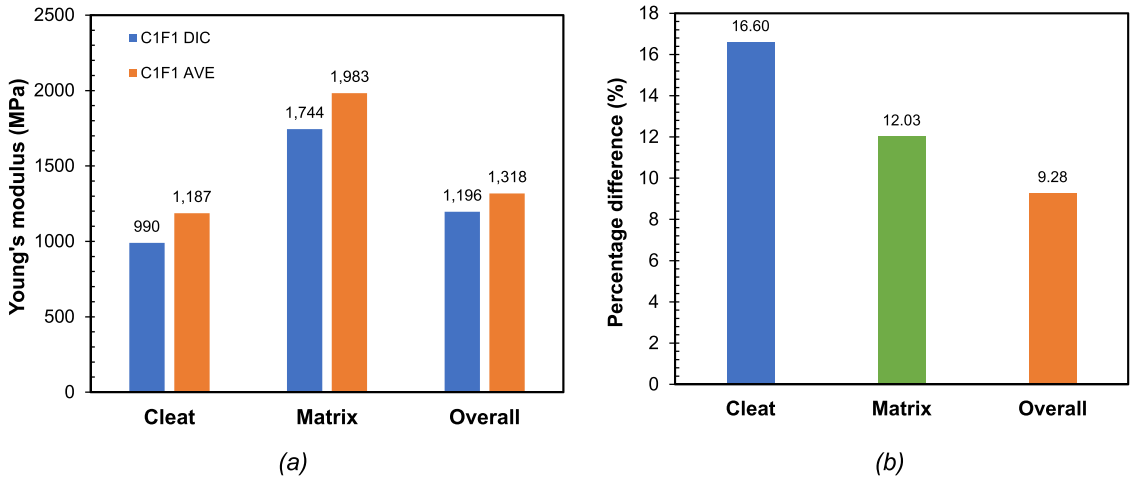

Fig. 13. (a) Average Young's modulus from all cycles (b) percentage difference of average Young's modulus between DIC and AVE.

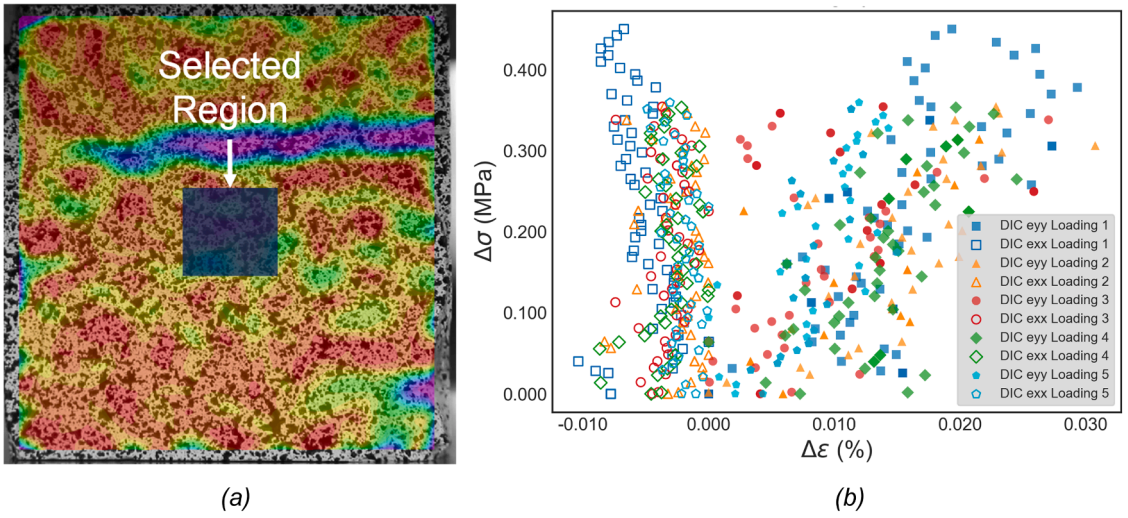

Fig. 14. Example illustration of Poisson's ratio analysis for sample C1F1 using the DIC method: (a) Selected region for Poisson's ratio analysis; (b) Stress and strain (ϵ_{xx} and ϵ_{yy}) data from different loading stages obtained through DIC analysis.

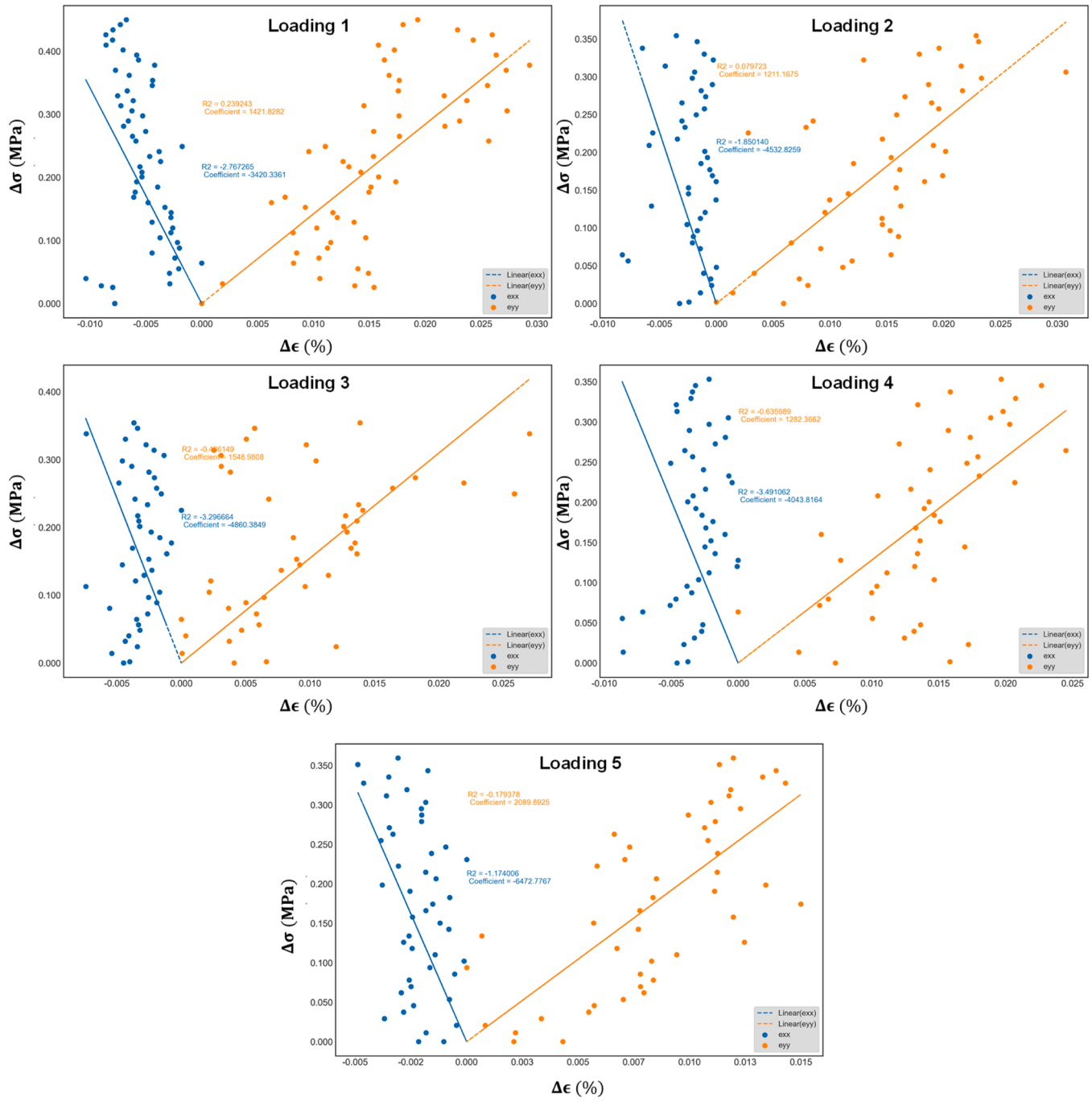

Fig. 15. C1F1 ϵ_{xx} Vs. ϵ_{yy}.

Table 4
C1F1 Poisson's ratio.

Loading Cycle	Poisson's ratio (C1F1)	Poisson's ratio (C1F2)
1	0.416	0.153
2	0.267	0.302
3	0.319	0.174
4	0.317	0.149
5	0.323	0.189
Average (each sample)	0.328	0.193
Average (all samples)	0.261	

set to 500 N/min, and the maximum load was limited to 950 N to maintain purely elastic deformation in the coal sample. Only a single loading cycle was performed for sample C2.

Fig. 9(a) presents the stress-strain curves obtained from both the DIC system and strain gauge measurements. The data shows strong agreement between the two methods, with both curves displaying linear stress-strain behavior, characteristic of elastic deformation. The linear regression analysis indicates a high correlation for both datasets, as reflected by the R^2 values (0.982 for the DIC system and 0.879 for the strain gauge).

Fig. 9(b) further validates the DIC system's accuracy by showing the percentage error between the DIC and strain gauge measurements across varying stress levels. The error decreases significantly as stress increases, stabilizing below 5 % at higher stress levels. This suggests that the DIC

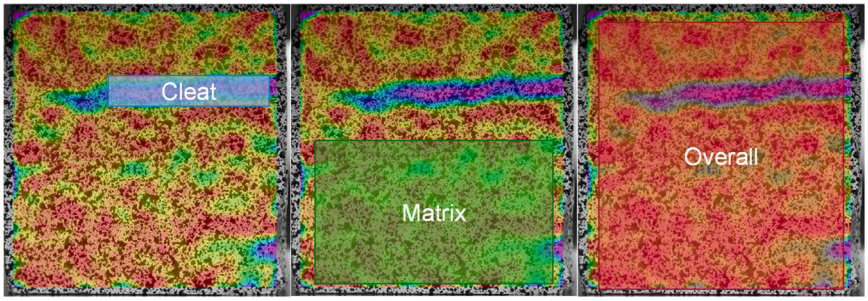

Fig. 16. Illustration of region selection for (a) cleat region (b) matrix region and (c) overall region for C1F1.

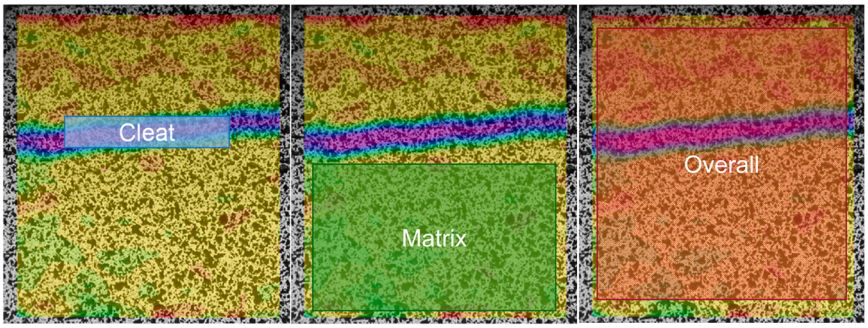

Fig. 17. Illustration of region selection for (a) cleat region (b) matrix region and (c) overall region for C1F2.

system maintains high precision, particularly in the mid-to-high stress range.

Overall, the close agreement between the DIC and strain gauge measurements confirms the reliability of the DIC system for capturing deformation in coal samples under elastic loading conditions.

3.2. DIC accuracy validation using AVE method

While the strain gauge method demonstrated good DIC accuracy in measuring coal deformation within the matrix region, it is unable to validate the deformation in the cleat and overall region due to its size limitations and lack of flexibility. Therefore, to validate the accuracy of the DIC method in the cleat, matrix, and overall region, the strain of sample C1 during the cyclic loading is measured using both the AVE and DIC methods separately and matched according to their positions. Fig. 10 illustrates the AVE points and DIC positions for sample C1F1 (cubic sample 1 face 1). Nine points were drawn on the coal surface for AVE strain analysis, and three sets of points 2–5, 5–8, and 2–8 were selected along the coal surface's center line, represented in Fig. 10 (a). These points correspond to cleat, matrix, and overall region in the DIC test, respectively, as illustrated in Fig. 10 (b). For the DIC analysis, the full-field surface strain is determined first, and then the averaged ε_{yy} along the selected line (Fig. 10 (b)) is calculated using Eq.(3) and Eq.(4).

Fig. 11 shows the stress-strain curve of DIC and AVE methods for each loading cycle. Blue dots represent the DIC results, and the orange dots represent the AVE results. The solid dots represent the matrix region, the empty dots represent the cleat region, and the dots with lighter colors represent the overall region, including the cleat and matrix region. The stress-strain curves for DIC and AVE are very close for every loading cycle, indicating that the DIC method gives an accurate result. Therefore, Young's modulus of the coal can now be calculated according to the stress-strain curve.

Fig. 12 summarizes Young's modulus for loading cycles shown in Fig. 11, and Fig. 13 (a) shows the averaged Young's modulus in the cleat, matrix and overall region for the DIC and AVE methods. For both AVE and DIC, $E_{cleat} < E_{overall} < E_{matrix}$, indicated the fracture inside a specimen can significantly reduce the overall Young's modulus. Fig. 13 (b) illustrates the percentage differences between the AVE and DIC methods. The results reveal a percentage difference of 16.60 % for the cleat region, 12.03 % for the matrix region, and 9.28 % for the overall region. These variations may arise from i) slight differences in the measurement regions between DIC and AVE and ii) minor discrepancies in elastic behavior during the two-stage compression tests. Thus, given the insignificant percentage difference, it can be concluded that the DIC method is a validated and reliable tool for accurately assessing surface deformation.

The following section determines the Poisson's ratio of samples C1F1 and C1F2. Since these two samples provide similar stress-strain graphs and results, only the C1F1 result is demonstrated. The center areas of C1F1 and C1F2 were selected for Poisson's ratio results validation as they did not have major fractures. Fig. 14 (a) shows the typical selected areas from sample C1F1 Poisson's ratio. While Fig. 14 (b) shows the stress-strain curve of ε_{xx} and ε_{yy} from each loading cycle. It can be seen that ε_{yy} are positive, indicating that the sample is in compression along y-axis (loading direction). ϵ_{yy} is negative, meaning that the sample is in tension along the x-axis.

Fig. 15 shows the stress-strain curve of ε_{xx} and ε_{yy} for each loading cycle. Linear regressions are applied to fit these data points, and the Poisson's ratio can be calculated using these linear fitted coefficients applying Eq.(14). The calculated Poisson's ratios are listed in Table 4. The Poisson's ratio for C1F1 varies slightly, with an average of 0.328. An average Poisson's ratio of 0.193 was obtained for C1F2. The obtained Poisson's ratio shows a good agreement with typical coal values for Bowen Basin [25].

3.3. Mechanical properties of coal cleat, matrix, and overall

This section quantifies the mechanical response of different coal

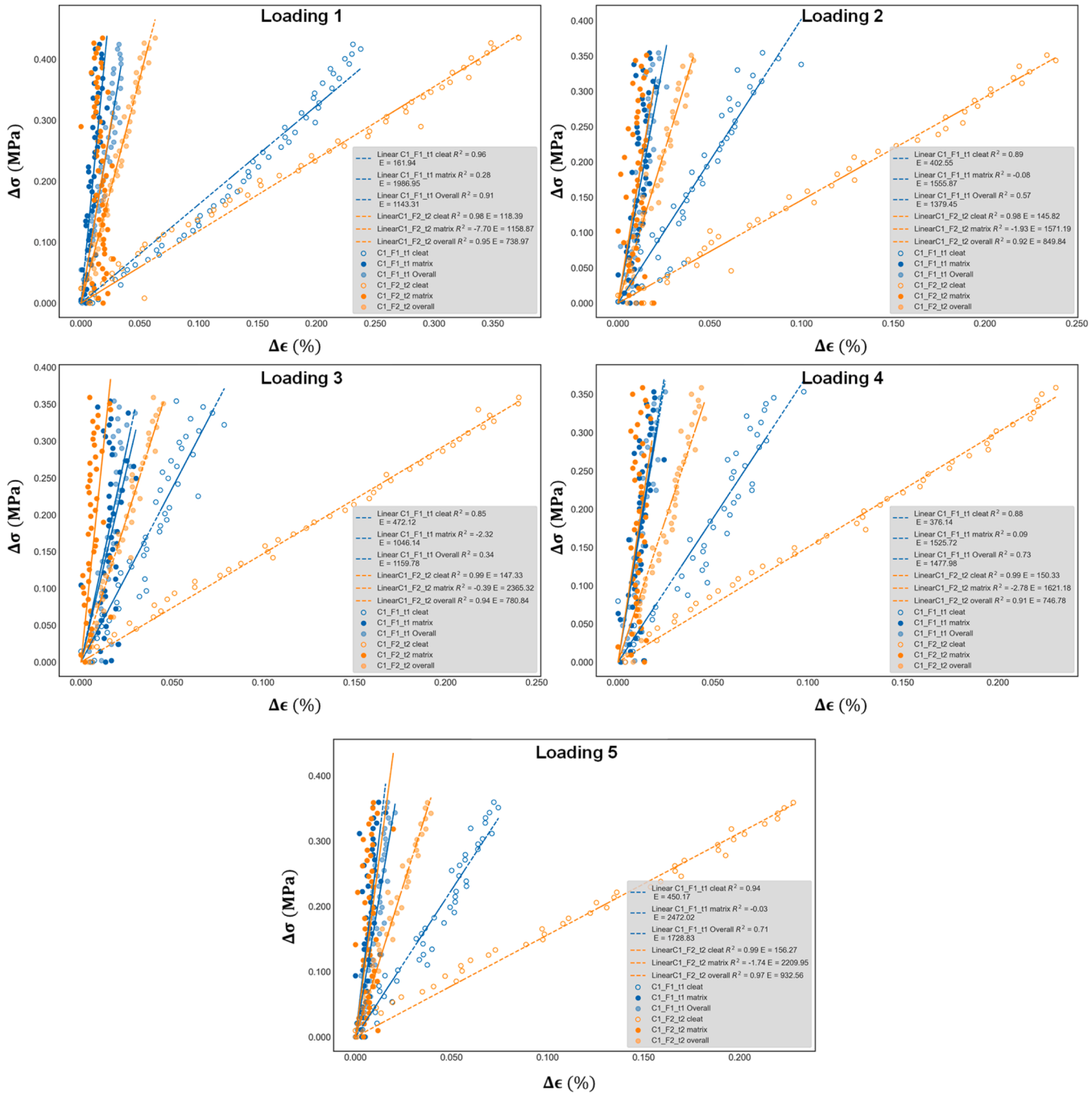

Fig. 18. Cleat Vs. matrix Vs. overall stress-strain curve for C1F1 and C1F2.

components (i.e., cleat, matrix, and bulk) to compression. The DIC results of C1F1 and C1F2 are compared with three regions (i.e., cleat region, matrix region and the overall region), as illustrated in Fig. 16 and Fig. 17. The stress-strain curves for each loading cycle are plotted in Fig. 18.

Eq. (5) was used to determine the Young's modulus for each region. For most regions and loading cycles, the linear regression proves an excellent R^2 value (>0.9). Fig. 19 summarized Young's modulus for selected regions for all loading cycles. It is observed for both C1F1 and C1F2 $E_{cleat} < E_{overall} < E_{matrix}$, suggesting that the fracture inside a specimen can significantly reduce the overall Young's modulus.

Fig. 20 (a) shows the Young's modulus of a selected region by averaging Young's modulus from each loading cycle. Fig. 20 (b) shows the percentage difference of these Young's moduli between C1F1 and C1F2. Results demonstrate that Young's moduli of the cleat region show a significant difference between C1F1 and C1F2 (159.41 % difference). This is due to the different aperture sizes of fractures. Young's moduli in the matrix region are almost identical for C1F1 and C1F2 (<3.81 % difference) since they are the different faces of the same sample. Furthermore, the overall Young's modulus of C1F2 shows a noticeable reduction (70.15 % difference) compared to C1F1 due to its lower cleat strength reducing its overall strength.

The average Young's modulus of the tested samples is 258 MPa for the cleat region (E_{cleat}), 1751 MPa for the matrix region (E_{matrix}), and 1094 MPa for the overall region ($E_{overall}$). The ratio of E_{cleat}: E_{matrix}: $E_{overall}$ is determined to be 0.24:1.60:1.00, reflecting the significant influence of cleat and matrix mechanical properties on the bulk behavior of coal.

The contributions of E_{matrix} and E_{cleat} to the overall Young's modulus

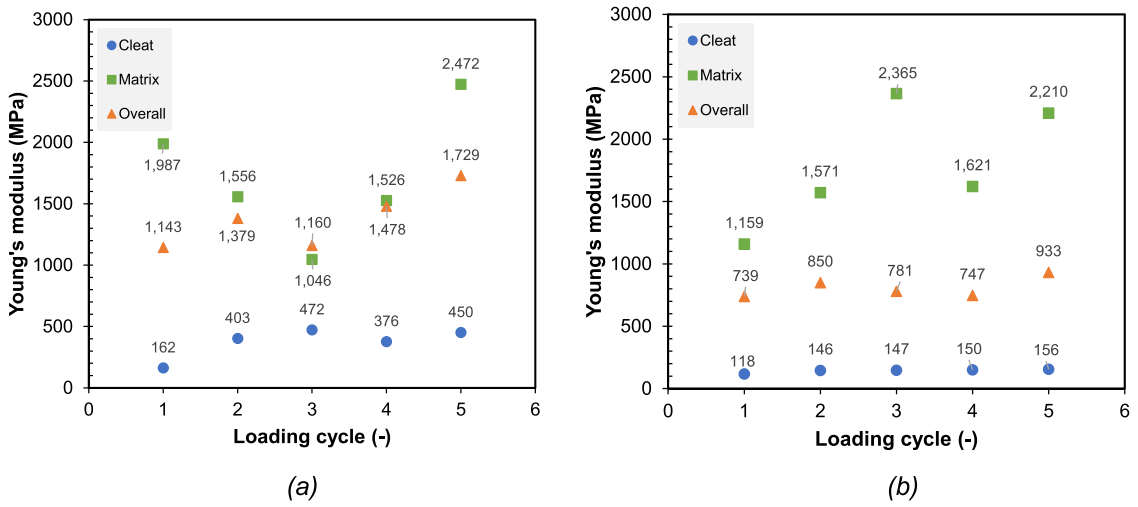

Fig. 19. Young's modulus for loading cycles a) C1F1, and b) C1F2.

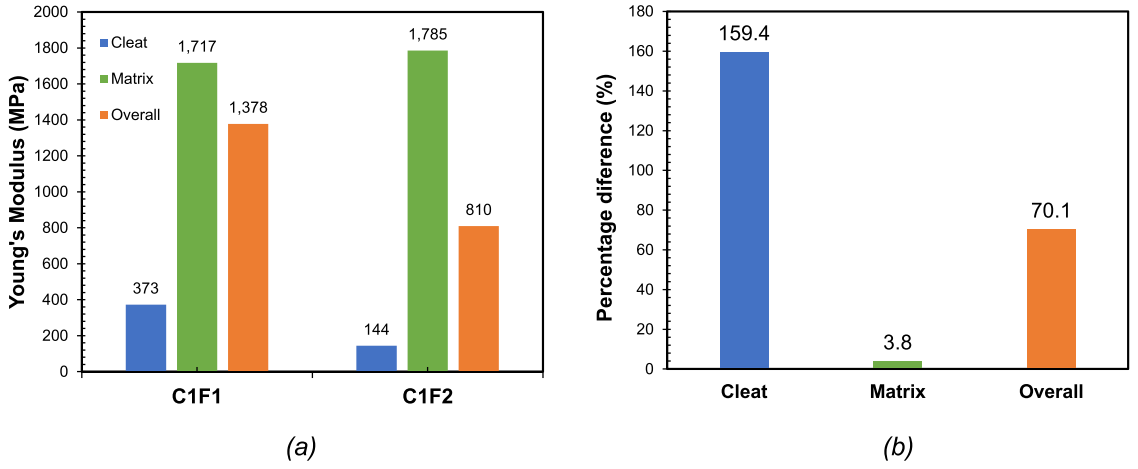

Fig. 20. (a) Averaged Young's modulus for C1F1 and C1F2, and (b) Variation of Young's modulus between C1F1 and C1F2.

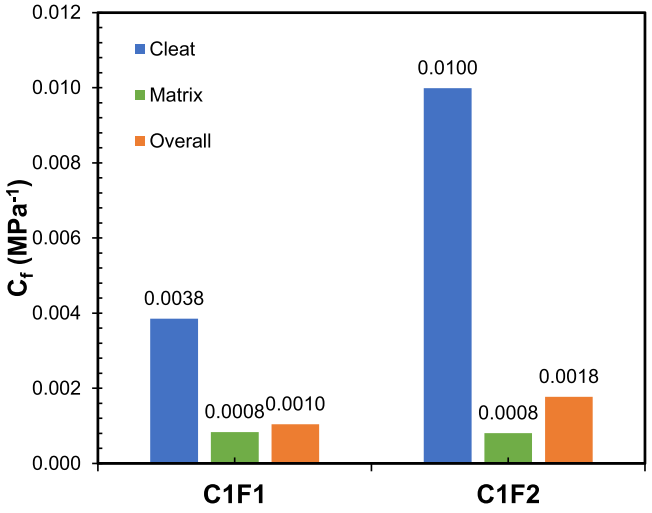

Fig. 21. Averaged cleat compressibility for C1F1 and C1F2.

$E_{overall}$ are essential for understanding the mechanical behavior of coal. This relationship is defined by the following equation:

$$E_{overall} = A \bullet E_{matrix} + (1 - A) \bullet E_{cleat} \tag{15}$$

Using the average Young's modulus values for the cleat (E_{cleat} = 258 MPa), matrix (E_{matrix} = 1751 MPa), and overall bulk coal ($E_{overall}$ = 1094 MPa), the matrix contribution (A) is calculated as 0.56, while the cleat contribution (1 - A) is 0.44.

This equation provides a practical tool for estimating $E_{overall}$ when E_{cleat} *and* E_{matrix} are known. Conversely, if the overall Young's modulus and one of the region's moduli are known, the other can be derived. However, it is crucial to recognize that the contributions of the matrix (A) and cleat (1 - A) can vary depending on factors such as cleat density and aperture size, which influence the mechanical response of the coal.

Cleat compressibility measures the response of a cleat network to changes in stress. It plays a vital role in modeling reservoir permeability and predicting permeability variations during coal seam gas recovery. The cleat compressibility C_f can be determined using the following equation:

$$C_f = \frac{3(1 - 2\nu)}{E} \tag{16}$$

where ν is the Piosson's ratio, and it is set to be 0.261, which is the averaged Piosson's ratio determined previously, E is the young's modulus. Fig. 21 shows the cleat compressibility of cleat, matrix and

overall region, which determined by applying Young's modulus in Fig. 20 (a) to Eq.(16). For both C1F1 and C1F2 samples, the cleat region exhibits the highest cleat compressibility, followed by the overall region, while the matrix region shows the lowest compressibility. This observation suggests that the cleat volume is more susceptible to compression under high-stress conditions compared to coal matrix.

The average compressibility for cleat, matrix and overall regions are 0.0069, 0.0008 and 0.0014 MPa^{-1}, respectively. The ratios of compressibility between the cleat, matrix, and overall regions are C_{cleat}: C_{matrix}: $C_{overall}$ = 4.24: 0.62: 1.00. These results indicate that the cleats are almost 5 times more compressible than the intact coal, which highlights their role as the primary contributors to deformation and permeability changes under stress. This behavior is critical for understanding fluid flow and mechanical behavior in coal seams, as cleat compressibility directly influences permeability and gas extraction efficiency in coalbed methane production.

4. Conclusions

This work introduces an attempt to quantify the areal deformation of coal cleat and matrix regions and their contributions to overall deformation using the 2D Digital Image Correlation method. The main findings drawn from this work are:

1. The accuracy of the DIC method was successfully validated against strain gauge and Advanced Video Extensometer (AVE) measurements, exhibiting small percentage differences: 5 % relative to the strain gauge, and 16.60 %, 12.03 %, and 9.28 % in the cleat, matrix, and overall regions, respectively, compared to AVE measurements. This demonstrates the reliability and robustness of the DIC method in quantifying deformation in cleated coal samples.
2. Poisson's ratios were determined for the tested sample, with averages ranging from 0.193 to 0.328. These values align closely with typical values for Bowen Basin, further supporting the reliability of the DIC method.
3. The DIC analysis revealed significant differences in Young's modulus among the cleat, matrix, and overall regions. The matrix region shows the highest value (up to 1785.3 MPa), and the cleat region is the lowest (as low as 143.6 MPa). For both samples, the trend $E_{cleat} < E_{overall} < E_{matrix}$ was consistent. On average, the Young's modulus of cleat, matrix and overall regions are 258 MPa, 1751 MPa and 1094 MPa, respectively. The ratio between cleat, matrix, and overall regions was determined as 0.24:1.60:1.00. The contribution of E_{matrix} and E_{cleat} to the overall Young's modulus $E_{overall}$ were calculated, with the matrix contributing 56 % (A = 0.56) and the cleat contributing 44 % ($1 - A$ = 0.44).
4. The cleat compressibility, calculated using Poisson's ratio and Young's modulus, shows that cleats are almost six times more compressible than the coal matrix, with a compressibility ratio of C_{cleat}: C_{matrix}: $C_{overall}$ = 4.24: 0.62: 1.00. This highlights the significant role of cleats in coal deformation and permeability changes under stress.

The DIC method offers an efficient and high-resolution approach for measuring Young's modulus and compressibility in coal's heterogeneous structure, overcoming the limitations of conventional point-based methods. It effectively captures full-field strain distributions, enabling detailed assessment of cleat and matrix regions and their contributions to bulk coal deformation. This study provides a quantitative comparison of cleat, matrix, and overall mechanical properties, offering new insights into the role of cleats in coal's geomechanical behavior.

Additionally, obtaining a standard-size cleated coal sample is challenging in practice due to its fragile nature. Given the mechanical properties of the intact coal matrix, Young's modulus ratio from this study can potentially be used as a guideline to predict the mechanical properties of bulk-cleated coal.

CRediT authorship contribution statement

Huang Yixiao: Writing – review & editing, Writing – original draft, Visualization, Validation, Methodology, Investigation, Formal analysis, Data curation. **Shi Zhang:** Writing – review & editing, Visualization, Validation, Methodology, Investigation, Formal analysis, Conceptualization. **Li Jimmy Xuekai:** Writing – review & editing, Visualization, Validation, Methodology, Investigation, Formal analysis. **Zhang Tiancheng:** Writing – review & editing, Visualization, Validation, Methodology, Investigation, Formal analysis. **Chen Zhongwei:** Writing – review & editing, Validation, Supervision, Software, Resources, Project administration, Methodology, Investigation, Formal analysis, Conceptualization.

Declaration of Competing Interest

The authors declare that they have no known competing financial interests or personal relationships that could have appeared to influence the work reported in this paper.

References

[1] L. Bin, Experimental study of coal considering directivity effect of bedding plane under Brazilian splitting and uniaxial compression, Chin. J. Rock. Mech. Eng. (2013).
[2] J. Chai, Y. Liu, Y. OuYang, D. Zhang, W. Du, Application of digital image correlation technique for the damage characteristic of rock-like specimens under uniaxial compression, Adv. Civ. Eng. 2020 (2020) 8857495, https://doi.org/10.1155/2020/8857495.
[3] H. Chen, B. Jiang, T. Chen, S. Xu, G. Zhu, Experimental study on ultrasonic velocity and anisotropy of tectonically deformed coal, Int. J. Coal Geol. 179 (2017) 242–252, https://doi.org/10.1016/j.coal.2017.06.003.
[4] R. Ďuriš, E. Babalová, Application of the digital image correlation and the strain gauge method for determination of the test sample material properties, in: A. Öchsner, H. Altenbach (Eds.), Engineering Design Applications VI: Structures, Materials and Processes, Springer Nature Switzerland, 2024, pp. 13–24, https://doi.org/10.1007/978-3-031-60920-6_2.
[5] X. Hao, W. Du, Y. Jiang, D. Tannant, Y. Zhao, Y. Guo, Influence of bedding and cleats on the mechanical properties of a hard coal, Arab. J. Geosci. 11 (9) (2018) 200, https://doi.org/10.1007/s12517-018-3541-3.
[6] G.M. Hassan, Digital Image Correlation for discontinuous displacement measurement using subset segmentation, Opt. Lasers Eng. 115 (2019) 208–216, https://doi.org/10.1016/j.optlaseng.2018.12.003.
[7] C.D. Hawkes, Assessing the mechanical stability of horizontal boreholes in coal, Can. Geotech. J. 44 (2007) 797–813.
[8] L. Hou, X. Liu, L. Liang, J. Xiong, P. Zhang, B. Xie, D. Li, Investigation of coal and rock geo-mechanical properties evaluation based on the fracture complexity and wave velocity, J. Nat. Gas. Sci. Eng. 75 (2020) 103133.
[9] T. Hou-z, The measurement and analysis and application on the mechanical property of coal seam, Geol. Prospect. (2000).
[10] Y. Huang, Z. Shi, T. Flottmann, D. Kuznetsov, V. Rudolph, C. Leonardi, Z. Chen, Experimental study of coal directional sorption-induced strain under different temperatures. Asia Pacific Unconventional Resources Technology Conference, Virtual, sixteenth ed., Unconventional Resources Technology Conference (URTeC), 2021, pp. 655–681 (10.15530/ap-urtec-2021-208345).
[11] INSTRON. 2021. AVE2 non-contacting video extensometer. In.
[12] H. Kong, L. Wang, G. Guoqing, B. Xu, Application of DICM on similar material simulation experiment for rock-like materials, Mater. Adv. Civ. Eng. 2018 (2018) 1–15.
[13] X. Liu, X. Wang, E. Wang, Z. Liu, X. Xu, Study on ultrasonic response to mechanical structure of coal under loading and unloading condition, Shock Vib. 2017 (2017) 7643451, https://doi.org/10.1155/2017/7643451.
[14] N. McCormick, J. Lord, Digital image correlation, Mater. Today 13 (12) (2010) 52–54, https://doi.org/10.1016/S1369-7021(10)70235-2.
[15] F. Nath, P.E. Salvati, M. Mokhtari, A. Seibi, A. Hayatdavoudi, Laboratory investigation of dynamic strain development in sandstone and carbonate rocks under diametrical compression using digital-image correlation, SPE J. 24 (01) (2018) 254–273, https://doi.org/10.2118/187515-pa.
[16] E. Özaslan, A. Yetgin, B. Acar, M.A. Güler, Damage mode identification of open hole composite laminates based on acoustic emission and digital image correlation methods, Compos. Struct. 274 (2021) 114299, https://doi.org/10.1016/j.compstruct.2021.114299.
[17] B. Pan, L. Tian, Advanced video extensometer for non-contact, real-time, high-accuracy strain measurement, Opt. Express 24 (17) (2016) 19082–19093, https://doi.org/10.1364/OE.24.019082.
[18] Shi, Z., Huang, Y., Flottman, T., Leonardi, C., Lu, M., & Chen, Z. 2023. Characterization of anisotropic geomechanical properties of australian bowen basin coals through nanoindentation and upscaling approaches. Day 2 Wed, November 15, 2023.

[19] N. Shukla, M.K. Mishra, Experimental evaluation of failure characteristics of coal using 2D digital image correlation approach, Arab. J. Geosci. 13 (20) (2020) 1060, https://doi.org/10.1007/s12517-020-06044-9.
[20] Y. Tang, H. Zhang, X. Guo, T. Ren, Literature survey and application of a full-field 3D-DIC technique to determine the damage characteristic of rock under triaxial compression, Int. J. Damage Mech. 31 (2022) 1082–1095.
[21] T. Tingjiang, W. Enyuan, W. Xiaoran, M. Liuzhu, Y. Wenli, Resistivity and damage of coal under cyclic loading and unloading, Eng. Geol. 323 (2023) 107234, https://doi.org/10.1016/j.enggeo.2023.107234.
[22] L. Wei, Q. Yuan, Y. Ren, D. Jiang, D. Zhang, Y. Liu, Y. Zou, S. Ren, Analysis of failure mechanics and energy evolution of sandstone under uniaxial loading based on dic technology, Front. Earth Sci. (2022).
[23] H.Z. Xing, Q.B. Zhang, D. Ruan, S. Dehkhoda, G.X. Lu, J. Zhao, Full-field measurement and fracture characterisations of rocks under dynamic loads using high-speed three-dimensional digital image correlation, Int. J. Impact Eng. 113 (2018) 61–72, https://doi.org/10.1016/j.ijimpeng.2017.11.011.
[24] Yang, X., Serati, M., & Buddery, P. 2024. Coal strength measurement by stereo digital image correlation.
[25] M. Zhang, R. Viljoen, W. Zhang, M. Jeffries, S. Beaney, W. Chen, Q. Wang, 2018, A novel workflow to model geomechanical properties using fracture coherence interpretation and density inversion in the rangal coal measures of the Bowen basin in Australia. In: Proceedings of the SPE Asia Pacific Oil and Gas Conference and Exhibition,.

Zhongwei Chen is an associate professor at the School of Mechanical and Mining Engineering in the University of Queensland. A/Prof Chen's research interests are in the areas of resources geomechanics, fluid transport in fractured porous media, and applications of machine learning to underground mining, unconventional gas extraction, CO2 sequestration, and hydrogen underground storage.